Earth and Planetary Science Letters 308 (2011) 277–283

Contents lists available at ScienceDirect

Earth and Planetary Science Letters

journal homepage: www.elsevier.com/locate/epsl

Initiation of the great M_w 9.0 Tohoku–Oki earthquake

Risheng Chu [a,b,*], Shengji Wei [a,b], Don V. Helmberger [a,b], Zhongwen Zhan [a,b], Lupei Zhu [c], Hiroo Kanamori [a,b]

[a] Seismological Laboratory, California Institute of Technology, Pasadena, CA 91125, USA
[b] Tectonic Observatory, California Institute of Technology, Pasadena, CA 91125, USA
[c] Department of Earth and Atmospheric Sciences, Saint Louis University, St. Louis, MO 63108, USA

ARTICLE INFO

Article history:
Received 3 June 2011
Received in revised form 27 June 2011
Accepted 28 June 2011
Available online 13 July 2011

Editor: P. Shearer

Keywords:
the 2011 Tohoku–Oki earthquake
earthquake source parameters
earthquake initiation

ABSTRACT

We determined the location, size, mechanism, and the frequency content of the first 4.0 s of the 2011 Tohoku–Oki earthquake. Since the beginning of this earthquake is very small, we develop a comparative approach against a near-by reference earthquake, the master event. We first determined the water depth near the master event using the differential timing between the water phase *pwP* reflected from the air–water interface and the depth phase *pP* reflected from the water–crust interface. Then we located the master event using the well-known ocean bathymetry in the area. After calibrating teleseismic arrays ($\Delta = 30°$ to $90°$) at short periods for timing and amplitude with respect to the master event, we were able to determine the initiation of the main event. It began as a small ($M_w = 4.9$) thrust event located at 38.19°N, 142.68°E at a depth of 21 km, and, a few seconds later, evolved into a slower extremely large slip event up-dip.

1. Introduction

The beginning of an earthquake is characterized by the hypocentral location, origin time, and other characteristics such as the size, mechanism, and frequency content (i.e., spectrum). The hypocenter of an earthquake is not only just a basic source parameter, but is also important for slip inversion and back projection studies because it serves as a reference point for the spatial distribution of slip and back-projection patterns (e.g. Kiser and Ishii, 2011; Lay et al., 2010), as will be shown later. The size, mechanism, and spectrum of the beginning have direct relevance to earthquake early warning (e.g. Allen and Kanamori, 2003) and the physics of earthquake nucleation (Ellsworth and Beroza, 1995).

Current finite-fault inversions and back-projection studies usually adopt the U.S. Geological Survey National Earthquake Information Center (NEIC) locations. The locations are routinely determined using *P* arrivals recorded at global stations. However, an inspection of broad-band seismograms of the 2011 M_w 9.0 Tohoku–Oki earthquake (hereafter also referred to as the mainshock) reveals that, similar to many large subduction-zone earthquakes (e.g. Lay et al., 2005), it begins with a "whimper" and grows rapidly into a devastating megathrust event. In fact, the beginning of *P* wave is so small at many stations that it is hard to pick arrival times on broadband records. Because of this, accurate determination of the mainshock hypocenter is very difficult with conventional location methods. For example, NEIC location errors are often as large as 40 km for offshore earthquakes (Engdahl et al., 1998).

The Japan Meteorological Agency (JMA) also produces an earthquake catalog for Japan area. Since JMA uses the most dense land-based seismic network in the world, with its stations distributed essentially north–south, their locations are believed to be good in the NS direction provided that there is no strong velocity variation in the north–south direction. Since the main structural variation is due to continent–ocean transition in the east–west direction, the velocity variation in the north–south direction is considered small. However, they use a one-dimensional (1-D) crust-mantle structure for locating earthquakes and the accuracy in east–west direction is questionable, especially for offshore events, because the structure varies significantly along the path normal to the coast. The epicentral locations of the mainshock determined by NEIC, JMA, and Zhao et al. (Dapeng Zhao, written communications, 2011) differ as much as 50 km (Fig. 1, Table 1). In Table 1, we included the GCMT solution to show the mechanism. The GCMT location is not to be compared with others because it is the centroid location instead of the hypocentral location.

The main objective of this study is to determine the hypocenter location, mechanism, magnitude, and spectrum of the beginning part of the 2011 Tohoku–Oki earthquake relative to a master event which occurred in the same area. The source characteristics of the master event are determined from detailed analyses of teleseismic body waves. Its epicenter is estimated from the water depth, which is

* Corresponding author.
E-mail address: risheng.chu@gmail.com (R. Chu).

0012-821X/$ – see front matter © 2011 Elsevier B.V. All rights reserved.
doi:10.1016/j.epsl.2011.06.031

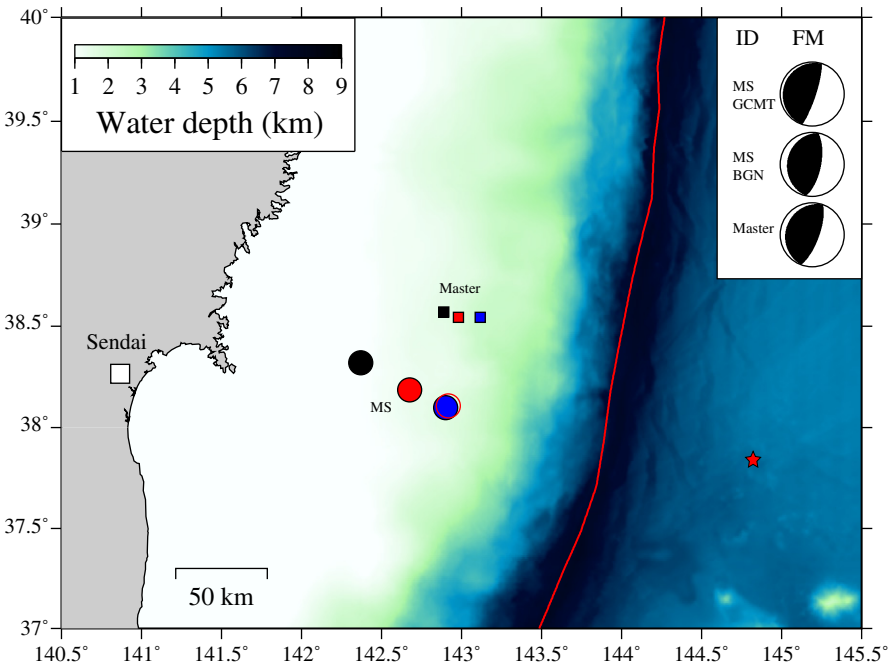

Fig. 1. Map of the off-shore epicentral region of the great 2011 Tohoku–Oki earthquake (circles) along with the 2008 master event (squares) and the 2011 outer-rise earthquake (red star). Black and blue symbols denote locations from the NEIC and JMA catalog, respectively. The red open circle represents the epicenter of the 2011 Tohoku–Oki earthquake by Zhao et al. (Dapeng Zhao, written communications, 2011). The red square denotes our preferred location of the master event determined by modeling teleseismic water waves. The red filled circle is the epicenter of the beginning of the mainshock determined relative to the master event. The 0.5-km bathymetric grid of the seafloor is obtained from the Japan Oceanographic Data Center. The red line denotes the trench (Bird, 2003). The inset displays the focal mechanisms of the mainshock (global CMT), the beginning of the mainshock (BGN), and the master earthquake, respectively.

determined from the differential travel times between teleseismic depth phases reflected from the bottom of the ocean and water phases reflected from the surface of the ocean.

2. Teleseismic water phase

Seismologists have long been aware of water phases (*pwP*) which are apparent for events beneath the ocean floor (Stewart and Helmberger, 1981; Ward, 1979). The dominant feature of water phases is "ringing" *P* waveforms at teleseismic distances (Fig. 2). This "ringing" feature is caused by *P*-wave energy trapped in the water layer because of the large velocity contrasts at the water–air interface and the water–crust interface (Fig. 2A). As an example of water phases, Fig. 2B shows a particularly clear observation of *pwP* for one of the aftershocks of the 2011 Tohoku–Oki earthquake which occurred on the outer-rise (03/11/2011, 22:51:19.8, M_w 5.5).

An automated Cut-and-Paste (CAP) method is used to search for the best-fitting mechanism for the outer-rise earthquake (Chu et al., 2011; Zhu and Helmberger, 1996). The near-source velocity model used for this event is modified from the results of seismic experiment in this area (Takahashi et al., 2004) with a uniform water depth of 5.5 km. Teleseismic waveforms from 178 stations of the global network are modeled at a frequency range of 0.3–2.0 Hz (Fig. S1). The mechanism is an oblique normal fault (Table 1). Note that for this mechanism, the phase *sP* is nodal at the USArray which greatly simplifies the waveforms.

In our present application, we need accurate measurements of the differential travel times between the *pwP* and *pP* phases. To this end we first explore the use of a dense array for identification of *pwP* phases. We align 417 recordings at USArray stations (Fig. 2C) on the *P* arrival and stack them using a bin size of 0.5°. We plot the observed and synthetic record section in Fig. 2B. The water phase after the 6th reflection (pw^6P) can still be observed. To further test sensitivity, we stacked the traces given in Fig. 2B over the ranges 75° to 85° to reduce the array to a single trace as displayed in Fig. 2D. This trace can then be compared with small changes in water depth. Synthetic tests suggest that the water phase *pwP* is sensitive to a change of water depth of 50 m, while the 3rd reflection (pw^3P) can detect a depth change of about 30 m for a uniform water depth (Fig. 2D). This example demonstrates that we can pick *pwP* phases accurately from a stacked record section obtained from a high-density array and the water depth can be determined with high precision as long as the bottom is relatively flat.

Unfortunately, due to the uniform water depth in the epicentral area of the outer-rise earthquake, we cannot locate this earthquake accurately from the water depth. However, since the result for the outer-rise earthquake is encouraging, we look for another event to be used as a master event.

Table 1
Earthquakes used in this study.

Orig. time	Lat (N)	Lon (E)	H (km)	M_w	Str/dip/rake	Source[a]
	38.57	142.89	16	5.3	210°/23°/94°	USGS
	38.54	143.12	17	5.3	204°/20°/90°	JMA[b]
2008/12/04, 03:10:57.8	38.58	143.21	31	5.3	192°/19°/81°	GCMT
	38.54	142.98	21	5.3	200°/18°/90°	This study
	38.30	142.37	20	9.0	187°/14°/68°	USGS
2011/03/11, 05:46:24.3	38.10	142.90	20	9.0	203°/10°/88°	JMA
	37.52	143.05	20	9.0	202°/10°/94°	GCMT
Beginning event	38.19	142.68	21	4.9	191°/23°/90°	This study
2011/03/11, 22:51:19.8	37.84	144.82	35	5.7	NA	USGS
	NA	NA	19	5.5	263°/56°/−31°	This study

[a] Earthquake information from all agencies is accessed on April 25, 2011.
[b] JMA's focal mechanism is from National Research Institute for Earth Science and Disaster Prevention (NIED).

3. The 2008 master event

Since we want to determine the hypocenter of the 2011 Tohoku–Oki earthquake with respect to a master event, an accurate

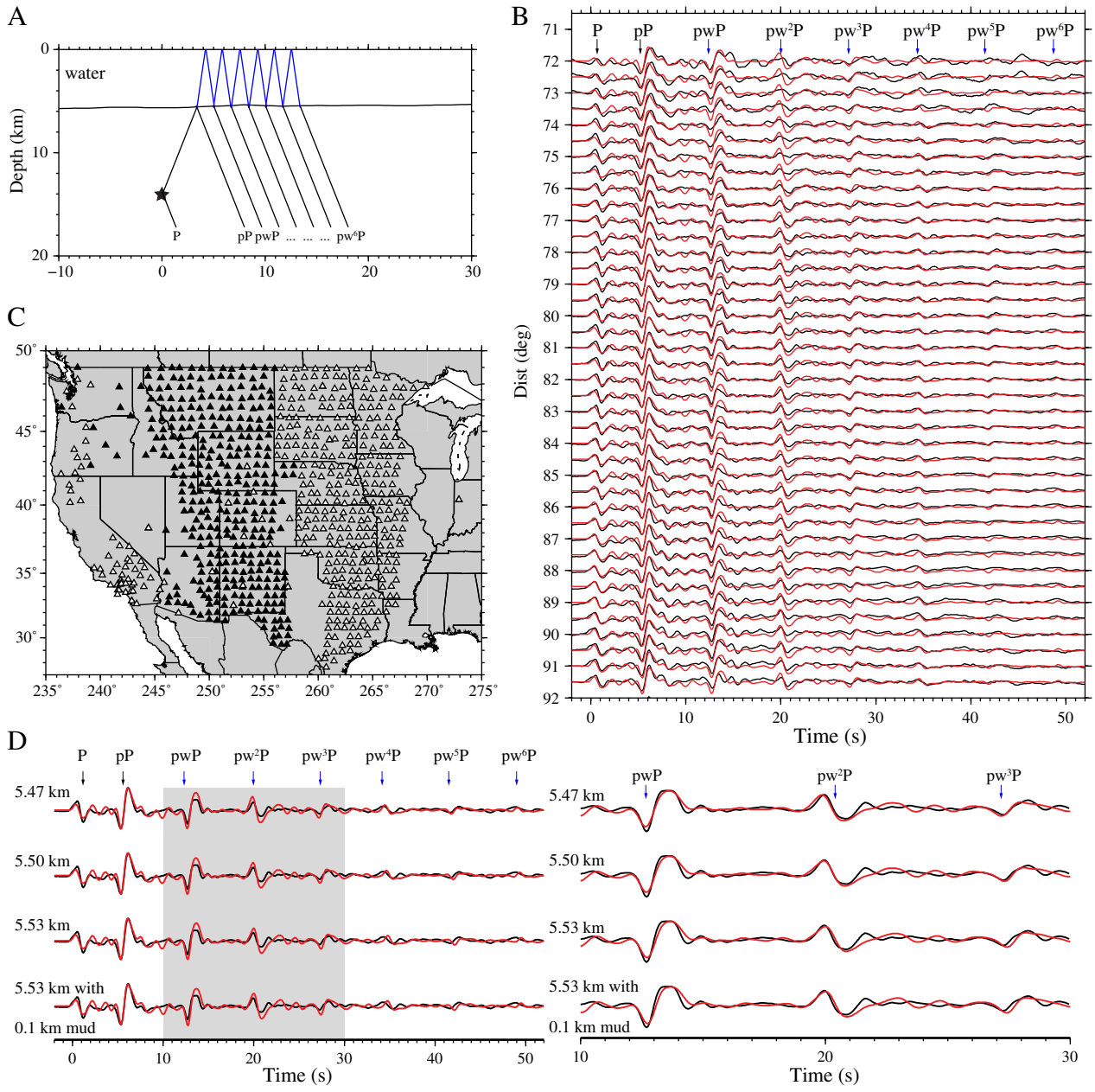

Fig. 2. Teleseismic water phases. (A) A sketch of the ray paths of teleseismic water phases. (B) Record section of the outer-rise earthquake recorded by USArray stations, 417 seismograms are stacked using a bin size of 0.5°. The depth phase *pP* and water phases are labeled on top with black and blue arrows, respectively. Synthetic seismograms (red) are calculated using a velocity model taken from Takahashi et al. (2004) with a uniform water depth of 5.5 km. (C) Map of the USArray stations recording the 03/11/2011 outer-rise earthquake (white triangles). Black triangles recorded the 2008 master event shown in Fig. 3. (D) Sensitivity test of water phases on water depth of 5.43 km, 5.50 km, and 5.53 km. In order to test the effect of ocean bottom sediment, we placed a 0.1 km mud layer with a *P* velocity of 2.0 km/s below a 5.53 km water layer. The sediment has no visual effect on the waveforms. Water phases to the 3rd reverberations are enlarged on the right. It is clear that the water depth is about 5.50 km.

hypocentral location of the master event is critical. As shown in Fig. 3A, the ocean bathymetry in the mainshock area varies rapidly in the EW direction and is relatively flat in the NS direction. On the other hand, the epicenters of the JMA catalog are believed to be located better in NS direction because of their wide station distribution in the NS direction. Thus, we can combine these two features to locate the master earthquake. Here, we fix the latitude of the epicenter at the JMA location, and determine only the longitude using water phases.

After having examined earthquakes with magnitude $5.0 \le M_w \le 5.5$ between 2008 and 2011 which are close to the 2011 Tohoku–Oki earthquake, we chose an earthquake (12/04/2008, Fig. 1 and Table 1) as our master event. The hypocentral parameters and the mechanism parameters of the master event taken from the NEIC catalog are listed in Table 1. This M_w 5.3 earthquake has a relatively simple source time function and good long-period waveforms at teleseismic distances, which are suitable for path calibration.

We determined the mechanism and depth of the master event by inversion of teleseismic waves from over 200 stations. Four examples are displayed in Fig. 3B. We cross-correlated waveforms of the observed and synthetic long-period *P* waves (0.02–0.1 Hz) and obtained a best-fit mechanism of (strike/dip/rake) = (200°/18°/90°) and a depth of 21 km (Fig. S2A–S2B). We then computed synthetic short-period (0.8–2.0 Hz) *P* waves for the master event using the hypocenter and mechanism determined above and cross-correlated

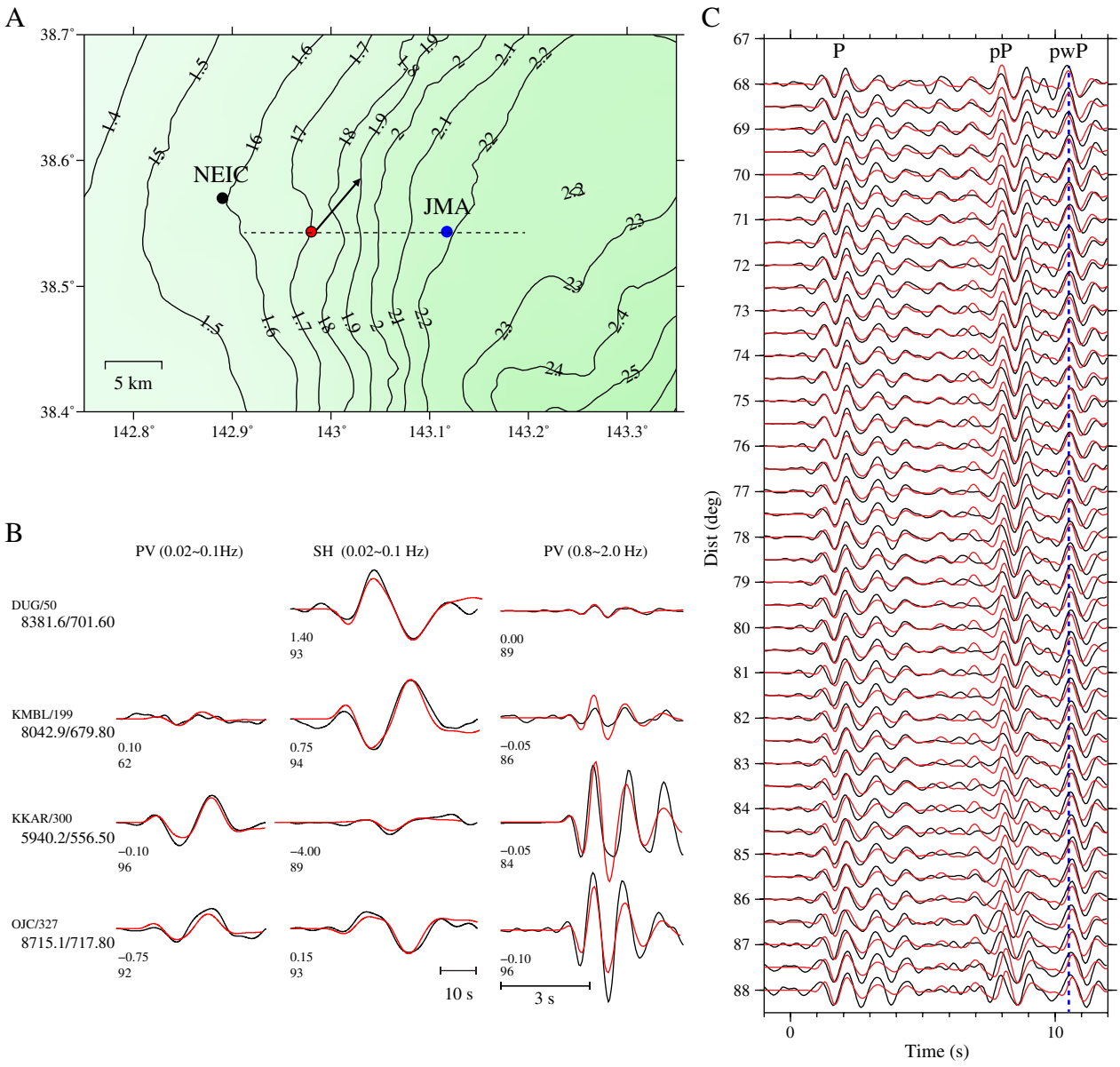

Fig. 3. Relocation of the 2008 master earthquake using differential depth phases. (A) Locations from NEIC and JMA catalogs are plotted as black and blue dots, respectively. The red dot represents the refined location. The arrows indicate the averaged azimuth of the USArray and the arrowhead represents the reflecting point of *pwP* at ocean surface. Black contours show water depth with an increase of 0.1 km. (B) Sample of waveform fits in the calibration of master event. We cut each seismogram into *P* and *SH* segments and allow a maximum shift of 5.0 s to find the best fits using the CAP method. The number after the station name is the azimuth. Two numbers below each station name are the epicentral distance in km and initial picked arrival time (tn). The two numbers below the seismogram are the time shift and cross-correlation coefficient (CCs) after inverting the waveforms. Accurate arrival times can be obtained by adding tn and the corresponding time shift from waveform fits. The earthquake has a thrust mechanism with strike/dip/rake of 200°/18°/90° and a depth of 21 km. Representative waveform fits are shown as data (black) and synthetics (red). We repeat the same procedure at a relatively high frequency of 0.8–2.0 Hz. Because depth phases are contaminated by complex structures above the earthquake, we only use direct *P* from 154 stations allowing a maximum shift of 0.5 s. Most of the waveform fits have CCs larger than 80% (Fig. S3). Path calibration for each station can be accurately obtained at this high frequency range. (C) Stacking of the waveforms recorded by USArray at a frequency range of 0.8–2.0 Hz is shown as black seismograms with *P*, *pP* and *pwP* phases labeled. Synthetic seismograms (red) are for the water depth of 1.9 km. We use JMA's latitude (dashed line in A) and a grid search in the EW direction is conducted to find this best location.

them with the observed. The cross-correlation coefficient is higher than 0.8 at about 75% of the stations (Fig. S2C), but the correlation is poor at the other 25% of the stations which is typical for comparisons of short-period data (Chu et al., 2011). The poor correlation is mainly due to high-amplitude background noise and site complexity. Time delays or shifts are noted to obtain a simple set of path-dependent travel-time corrections for the 1-D model. Also, the amplitudes are adjusted with Amplitude Amplification Factors (AAFs) to correct for path-dependent attenuation and site response relative to the 1-D model (Fig. S3), see Tan and Helmberger (2007) for details.

Similar to the outer-rise earthquake, we analyzed the water phases at USArray for the master event. Since the earthquake is small and *P* waves are close to nodal at USArray, we filtered the waveforms at a frequency band of 0.8–2.0 Hz. Fig. 3C shows the result. The result is less clear than that for the outer-rise event because of a weaker *pP* and stronger *sP* and of a somewhat more complex ocean bathymetry. Nevertheless, as shown in Fig. 3C, we can accurately determine the differential times between the depth phase *pP* and the water phase *pwP*. We can estimate the water depth at the reflection point to be 1.9 km from which we can determine using Fig. 3A an epicenter of

38.54°N and 142.98°E. Short-period seismic arrays at other azimuths support this location as shown in Fig. S4.

4. Location of the 2011 Tohoku–Oki earthquake

Having established the location and the mechanism of the master event, we now attempt to locate the beginning of the mainshock relative to the master event. Because the mechanism of the mainshock determined by the global CMT inversion is similar to that of the master event (Fig. 1), we expect that the waveforms of short-period *P* waves of the mainshock and the master event to be similar except for small time shifts due to their different locations. Since the beginning of the mainshock is very small on broad-band or long-period records, we compare the short-period (0.8–2.0 Hz) *P* waves from the master event and the mainshock for the purpose of relocation. As shown in Fig. 4A and B, we see very similar waveforms between the master event and the first 4.0 s of the mainshock. From this comparison, we can refine its mechanism and locate the beginning of the mainshock.

In order to obtain the mechanism of the beginning of the mainshock, we first hand-pick the arrivals of interest by examining the record sections using the NEIC location. Fig. 4A displays a few examples. In the first 4.0 s of the waveforms, the depth phases are not present. Although we invert the mechanism at relatively high frequency (0.8–2.0 Hz), the teleseismic path effects can be considered reliable as demonstrated in Chu et al. (2011). Thus the amplitude corrections from the master event (AAFs) are applied to each station before the inversion. We then use the CAP method to determine the focal mechanism using a time window of 4.0 s and a maximum shift of 1.0 s to obtain the best fit. A few examples are displayed in Fig. 4C. The best-fit mechanism (strike/dip/rake = 191°/23°/90°, Fig. S5) is similar to that given by NEIC (Fig. 1). In order to test the uncertainty of our focal mechanism, we randomly pick 50 stations and invert the focal mechanism of the beginning event. We repeat the procedure 200 times and obtain a stable solution (Fig. S6). *P* arrival times at each station can be accurately determined by cross-correlating the observed data with synthetics. Its travel-time residuals are shown in Fig. S7. We then use the time differences of the *P* waves between the mainshock and the master event as a function of azimuth to locate the beginning of the mainshock relative to the master event (Fig. 4D). The method is similar to the double-difference relocation algorithm (Waldhauser and Ellsworth, 2000) except that we correct for mechanism. We locate the beginning of the mainshock at a latitude of 38.19°N, and a longitude of 142.68°E. With this location we can match the onset of the mainshock and the master event very well, as shown in Fig. 4B. The root-mean-square (RMS) of the time differences is reduced from 3.5 s to 0.4 s (Fig. 4D).

For the determination of the depth, we assume that the mainshock nucleated on the plate boundary, and use the plate boundary interface geometry. The eastern Honshu area has been extensively studied by

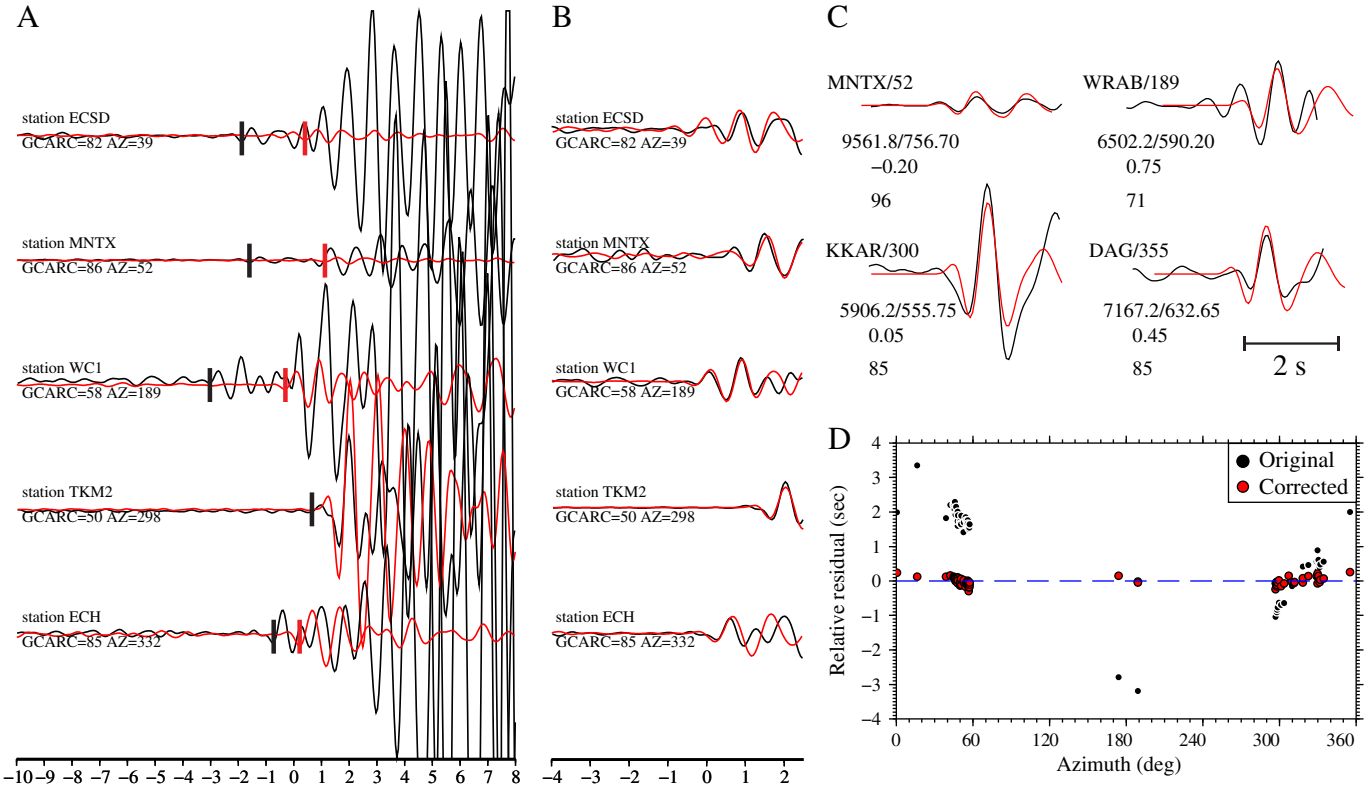

Fig. 4. Focal mechanism and location of the beginning of the main rupture. (A) Comparison of waveforms at 0.8–2.0 Hz for the mainshock (black) and the master earthquake (red) for a sample of 5 teleseismic stations. All seismograms are aligned with IASPEI91 predictions using the refined location for the master event and the NEIC location for the mainshock. Since the beginning of the mainshock has a magnitude 0.4 smaller than the master event, all black traces are multiplied by 2 for display purposes. Black and red vertical bars denote the arrival time of the mainshock and master event, respectively. (B) Comparison of data for the first 2.5 s from these two earthquakes aligned with IASPEI91 predictions. The seismograms are normalized to the maximum amplitudes. The epicenter of the mainshock is at the refined location. Waveforms from the master earthquake and the mainshock match very well, which confirms the accuracy of the refined location. (C) The first 4.0 s of 82 recordings with relatively low noise levels were used in the CAP inversion with 4 examples displayed. Each seismogram has been corrected by the AAFs from the master event. A maximum shift of 1.0 s is allowed and the solution with strike/dip/rake at 191°/23°/90° is obtained, see Fig. 3 for more details. (D) Relative travel-time residuals of the mainshock with respect to the master event are shown as black dots. Red dots denote residuals corrected with respect to the new location given as the red star in Fig. 1.

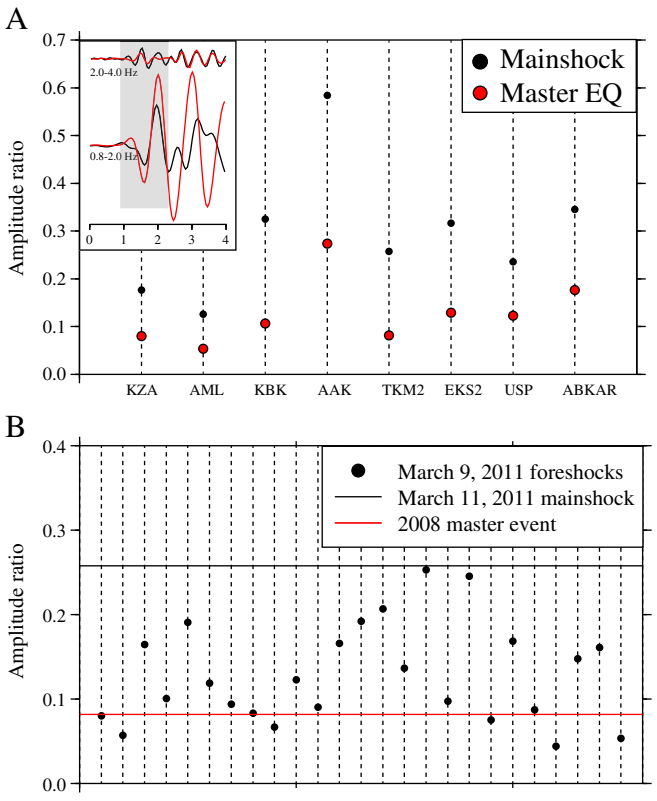

Fig. 5. (A) High-frequency (2.0–4.0 Hz) to low-frequency (0.8–2.0 Hz) amplitude ratio for the master earthquake (red dots) and the beginning of the mainshock (black dots) at 8 stations (x-axis). The inset shows an example time window for the measurements at station TKM2. (B) Comparison of high-frequency/low-frequency amplitude ratio for station TKM2 recording the 03/09/2011 foreshock sequence. Each dot represents an earthquake. The ratios for master earthquake and beginning of the mainshock are plotted as red line and black line, respectively.

various investigators (e.g. Miura et al., 2005; Takahashi et al., 2004), and the subduction slab geometry is better known than in any other area in the world. Using the result of most recent compilation (Simons et al., 2011), we estimate that the 2011 earthquake nucleated at a depth of 21 km.

5. Frequency content

Now we examine the frequency content of the *P* wave of the master event and the beginning of the mainshock. Since we cannot isolate the beginning part of the mainshock, we cannot determine the spectrum. Thus, we just measure the amplitude at two frequency bands. Let A_{hi} and A_{lo} be the amplitudes at high and low frequency bands, respectively. We choose the lower frequency band from 0.8 to 2.0 Hz with central frequency (f_{lo}) of 1.4 Hz and the higher frequency band from 2.0 to 4.0 Hz with central frequency (f_{hi}) of 3.0 Hz. We measure A_{hi} and A_{lo} for the master event and the beginning of the mainshock from the records of 8 stations which have good signals at both frequency bands. Fig. 5A shows the ratios A_{hi}/A_{lo} for these 8 stations. The average ratios are 0.26 for the beginning of the mainshock and 0.09 for the master event. Since the magnitudes of both the beginning of the mainshock and the master event are about Mw = 5.0, the corner frequency is about 0.7 Hz so that the frequencies we are using here are above the corner frequency. For an omega square model, the amplitude ratio is given approximately by $(f_{lo}/f_{hi})^2 = 0.22$, which is approximately the same as that for the beginning of the main shock. Thus, this suggests that the spectrum of the beginning of the mainshock is similar to what is expected of the ordinary omega square model. The master event is deficient in high frequency by a factor of 3. For further comparison, Fig. 5B shows the ratios computed for the 25 Mw ≤ 5.3 aftershocks of the 3/9/2011 foreshock using the records at station TKM2. The ratios vary between the values for the master event and the beginning of the mainshock.

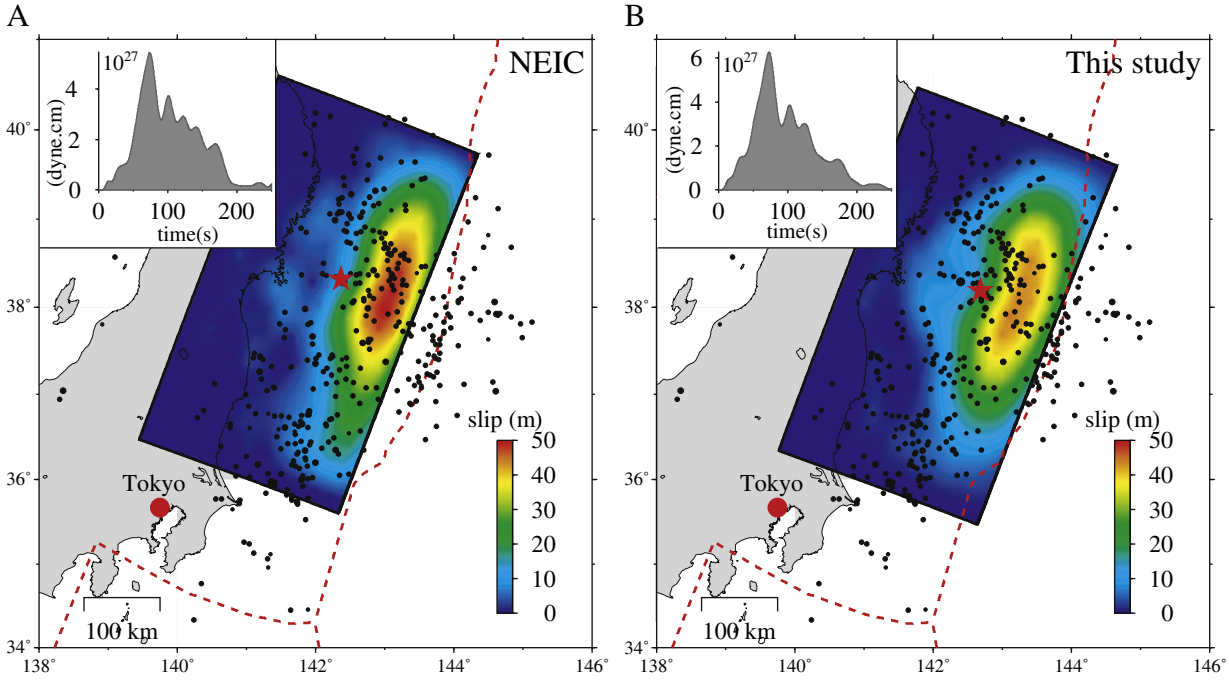

Fig. 6. Sensitivity of slip models obtained by combining GPS and teleseismic *P*-waveform data to the choice of the epicenter. The two slip models are developed with our epicenter location (A) and the NEIC location (B), respectively. Epicenter location is the only difference between the setup of these two inversions. Here, we use the global CMT solution to define the dip (10°) and strike (203°) of the fault plane. Moment-rate plot is inserted in the upper left of each panel. Red stars indicate the epicenters and black dots are aftershocks occurring in the first three days. Red dashed lines denote the plate boundaries (Bird, 2003).

6. Discussion and conclusion

An accurate location of the hypocenter is important for slip inversion and back projection studies. In these studies the rupture patterns are determined with relative to the rupture nucleation point, i.e. hypocenter. For example, Fig. 6 compares the slip pattern of the 2011 Tohoku–Oki earthquake determined from teleseismic body waves and GPS, using the NEIC hypocenter and that determined in this study. Since the epicenter is used as the initiation point of rupture, the entire pattern is displaced as much as 20 km to the east as our epicenter moves east from the NEIC epicenter. Also, because of the changes in the depth, some details of the slip distribution and the moment-rate function change. The exact location of the slip is important because it controls the tsunami excitation. A similar effect can be seen for the back-projection images presented in Simons et al. (2011); the entire pattern is shifted to the east by 20 km from the location given in Meng et al. (2011).

The physical characteristics of the beginning of the rupture also have important implications for how the 2011 Tohoku–Oki earthquake nucleated. Comparison of the high-frequency (0.8–4.0 Hz) energy radiated from the 2010 Maule earthquake and the 2011 Tohoku–Oki earthquake suggests that the 2011 Tohoku–Oki earthquake as a whole is deficient in high-frequency energy, after the magnitude difference is corrected for (Simons et al., 2011). Simons et al. (2011) also found that the largest slip which occurred along the trench is relatively slow similar to tsunami earthquakes (Polet and Kanamori, 2000). However, our result shows that the very beginning is not particularly slow suggesting that the 2011 Tohoku–Oki earthquake started as a regular small earthquake but triggered large amounts of slow slip in the up-dip portion of the plate boundary (Simons et al., 2011). Since our analysis is only for the 2011 Tohoku earthquake, we cannot make a general conclusion on the nucleation process of very large earthquakes. However, our observation suggests that the beginning of the Tohoku–Oki earthquake is just a small ($Mw = 4.9$) earthquake rather than some special nucleation process with a characteristic length and timescale that controls the final size of an earthquake, as suggested by several investigators (e.g., Ellsworth and Beroza, 1995; Iio, 1992, 1995).

In summary, we used teleseismically observed ocean reverberations to estimate the water depth from which we located the 2008 master earthquake in the off-shore direction. Global teleseismic path effects of travel time and amplitude are calibrated using the well-resolved source solutions of the master event. After applying the calibrations to the first 4.0 s of the 2011 Tohoku–Oki earthquake, we are able to determine the initial location and mechanism of the beginning of the event, which is an $Mw = 4.9$ thrust event at 38.19°N, 142.68°E at a depth of 21 km.

Supplementary materials related to this article can be found online at doi:10.1016/j.epsl.2011.06.031.

Acknowledgments

We would like to thank two anonymous reviewers. Their suggestions and comments made significant improvements to the manuscript. This work was partially supported by the Gordon and Betty Moore Foundation. RC and DVH are partially supported by the National Science Foundation through grant number EAR-0636012. Contribution 10062 of Seismological Laboratory, California Institute of Technology.

References

Allen, R.M., Kanamori, H., 2003. The potential for earthquake early warning in southern California. Science 300, 786–789.
Bird, P., 2003. An updated digital model of plate boundaries. Geochem. Geophys. Geosyst. 4 (3).
Chu, R., Ni, S., Pitarka, A., Helmberger, D.V., 2011. Inversion of source parameters for moderate earthquakes using short-period teleseismic P waves. Geophys. J. Int. in revision.
Ellsworth, W.L., Beroza, G.C., 1995. Seismic evidence for an earthquake nucleation phase. Science 268, 851–855.
Engdahl, E.R., van der Hilst, R., Buland, R., 1998. Global teleseismic earthquake relocation with improved travel times and procedures for depth determination. Bull. Seismol. Soc. Am. 88 (3), 722–743.
Iio, Y., 1992. Slow initial phase of the P-wave velocity pulse generated by microearthquakes. Geophys. Res. Lett. 19, 477–480.
Iio, Y., 1995. Observations of the slow initial phase generated by microearthquakes: implicationsfor earthquake nucleation and propagation. J. Geophys. Res. 100, 15333–15349.
Kiser, E., Ishii, M., 2011. The 2010 Mw 8.8 Chile earthquake: triggering on multiple segments and frequency-dependent rupture behavior. Geophys. Res. Lett. 38, L07301. doi:10.1029/2011GL047140.
Lay, T., Kanamori, H., Ammon, C.J., Nettles, M., Ward, S.N., Aster, R.C., Beck, S.L., Bilek, S.L., Brudzinski, M.R., Butler, R., DeShon, H.R., Ekström, G., Satake, K., Sipkin, S., 2005. The great Sumatra–Andaman earthquake of 26 December 2004. Science 308. doi:10.1126/science.1112250.
Lay, T., Ammon, C.J., Kanamori, H., Koper, K.D., Sufri, O., Hutko, A.R., 2010. Teleseismic inversion for rupture process of the 27 February 2010 Chile (Mw 8.8) earthquake. Geophys. Res. Lett. 37, L13301. doi:10.1029/2010GL043379.
Meng, L., Ampuero, J., Inbal, A., 2011. Rupture complexity of the 2011 M9 Tohoku-Oki earthquake revealed by high-resolution seismic array processing. 2011 SSA Annual Meeting, Memphis, USA.
Miura, S., Takahashi, N., Nakanishi, A., Tsuru, T., Kodaira, S., Kaneda, Y., 2005. Structural characteristics off Miyagi forearc region, the Japan Trench seismogenic zone, deduced from a wide-angle reflection and refraction study. Tectonophysics 407, 165–188.
Polet, J., Kanamori, H., 2000. Shallow subduction zone earthquakes and their tsunamigenic potential. Geophys. J. Int. 142, 684–702.
Simons, M., Sladen, A., Owen, S.E., Minson, S.E., Ortega, F., Jiang, J., Meng, L., Ampuero, J.-P., Wei, S., Chu, R., Helmberger, D.V., Kanamori, H., Hetland, E., Moore, A.W., Webb, F.H., 2011. The 2011 magnitude 9.0 Tohoku–Oki earthquake: mosaicking the megathrust from seconds to centuries. Science 332. doi:10.1126/science.1206731.
Stewart, G.S., Helmberger, D.V., 1981. The Bermuda earthquake of March 24, 1978: a significant oceanic intraplate event. J. Geophys. Res. 86 (B8), 7027–7036.
Takahashi, N., Kodaira, S., Tsuru, T., Park, J.-O., Kaneda, Y., Suyehiro, K., Kinoshita, H., Abe, S., Nishino, M., Hino, R., 2004. Seismic structure and seismogenesis off Sanriku region, northeastern Japan. Geophys. J. Int. 159, 129–145.
Tan, Y., Helmberger, D.V., 2007. A new method for determining small earthquake source parameters using short-period P waves. Bull. Seismol. Soc. Am. 97, 1176–1195.
Waldhauser, F., Ellsworth, W.L., 2000. A double-difference earthquake location algorithm: method and application to the Northern Hayward Fault, California. Bull. Seismol. Soc. Am. 90 (6), 1353–1368.
Ward, S., 1979. Ringing P waves and submarine faulting. J. Geophys. Res. 84, 3057–3062.
Zhu, L., Helmberger, D.V., 1996. Advancement in source estimation techniques using broadband regional seismograms. Bull. Seismol. Soc. Am. 86, 1634–1641.